Published in final edited form as:

Bone Joint J. 2019 July ; 101-B(7 SUPPLE C): 108–114. doi:10.1302/0301-620X.101B7.BJJ-2018-1473.R1.

Vascular endothelial growth factor pathway promotes osseointegration and CD31^{hi}EMCN^{hi} endothelium expansion in a mouse tibial implant model:

AN ANIMAL STUDY

G. Ji, MD [Assistant Professor],
Department of Joint Surgery, The Third Hospital of Hebei Medical University, Shijiazhuang, China; Research Division, Hospital for Special Surgery, New York, New York, USA.

R. Xu, PhD [Professor],
Department of Orthopedics, Xiang'an Hospital and State Key Laboratory of Cellular Stress Biology, School of Medicine, Xiamen University, Xiamen, China.

Y. Niu, MD [Research Fellow],
Department of Joint Surgery, The Third Hospital of Hebei Medical University, Shijiazhuang, China; Research Division, Hospital for Special Surgery, New York, New York, USA.

N. Li, PhD [Assistant Professor],
Department of Orthopedics, Xiang'an Hospital and State Key Laboratory of Cellular Stress Biology, School of Medicine, Xiamen University, Xiamen, China.

L. Ivashkiv, MD [Professor],
Research Division, Hospital for Special Surgery, New York, New York, USA.

M. P. G. Bostrom, MD, FACS [Professor],
Research Division, Hospital for Special Surgery, New York, New York, USA; Division of Adult Reconstruction and Joint Replacement, Department of Orthopaedic Surgery, Hospital for Special Surgery, New York, New York, USA.

M. B. Greenblatt, MD, PhD [Assistant Professor],

Correspondence should be sent to X. Yang; yangx@hss.edu.

Author contributions:
G. Ji: Designed the experiments, Performed most of the experiments, Wrote the manuscript.
R. Xu: Designed the experiments, Assisted with the flow cytometry analysis and cell sorting.
Y. Niu: Assisted with the mouse experiments.
N. Li: Assisted with the mouse experiments.
L. Ivashkiv: Assisted with the study design and data interpretation.
M. P. G. Bostrom: Assisted with the study design and data interpretation.
M. B. Greenblatt: Assisted with the study design and data interpretation; Edited the manuscript.
X. Yang: Designed and supervised the project; Wrote the manuscript.
G. Ji and R. Xu contributed equally to this work.

Ethical review statement:
This study was approved by the Institutional Animal Care and Use Committee of Hospital for Special Surgery.

This article was primary edited by G. Scott.

This paper was presented at The Knee Society 2018 Members Meeting in St. Louis, Missouri, United States.

Department of Pathology and Laboratory Medicine, Weill Cornell Medical College, Cornell University, New York, New York, USA; Assistant Scientist, Research Division, Hospital for Special Surgery, New York, New York, USA.

X. Yang, MD, MS [Assistant Scientist]
Research Division, Hospital for Special Surgery, New York, New York, USA.

Abstract

Aims—It is increasingly appreciated that coordinated regulation of angiogenesis and osteogenesis is needed for bone formation. How this regulation is achieved during peri-implant bone healing, such as osseointegration, is largely unclear. This study examined the relationship between angiogenesis and osteogenesis in a unique model of osseointegration of a mouse tibial implant by pharmacologically blocking the vascular endothelial growth factor (VEGF) pathway.

Materials and Methods—An implant was inserted into the right tibia of 16-week-old female C57BL/6 mice (n = 38). Mice received anti-VEGF receptor-1 (VEGFR-1) antibody (25 mg/kg) and VEGF receptor-2 (VEGFR-2) antibody (25 mg/kg; n = 19) or an isotype control antibody (n = 19). Flow cytometric (n = 4/group) and immunofluorescent (n = 3/group) analyses were performedat two weeks post-implantation to detect the distribution and density of $CD31^{hi}EMCN^{hi}$ endothelium. RNA sequencing analysis was performed using sorted $CD31^{hi}EMCN^{hi}$ endothelial cells (n = 2/group). Osteoblast lineage cells expressing osterix (OSX) and osteopontin (OPN) were also detected with immunofluorescence. Mechanical pull-out testing (n = 12/group) was used at four weeks post-implantation to determine the strength of the bone-implant interface. After pull-out testing, the tissue attached to the implant surface was harvested. Whole mount immunofluorescent staining of OSX and OPN was performed to determine the amount of osteoblast lineage cells.

Results—Flow cytometry revealed that anti-VEGFR treatment decreased $CD31^{hi}EMCN^{hi}$ vascular endothelium in the peri-implant bone *versus* controls at two weeks post-implantation. This was confirmed by the decrease of CD31 and endomucin (EMCN) double-positive cells detected with immunofluorescence. In addition, treated mice had more OPN-positive cells in both peri-implant bone and tissue on the implant surface at two weeks and four weeks, respectively. More OSX-positive cells were present in peri-implant bone at two weeks. More importantly, anti-VEGFR treatment decreased the maximum load of pull-out testing compared with the control.

Conclusion—VEGF pathway controls the coupling of angiogenesis and osteogenesis in orthopaedic implant osseointegration by affecting the formation of $CD31^{hi}EMCN^{hi}$ endothelium.

It is increasingly appreciated that the cementless joint arthroplasty can preserve bone stock, increase the ease of revision, and avoid cement fatigue and bone-cement interface failure.[1,2] The long-term survival and success of cementless implants requires osseointegration, which is the structural and functional connection between the bone and implant.[3] Early osseointegration and primary stability play a critical role in cementless joint arthroplasty and depend on predictable biological responses to foreign materials and incorporation of the endosseous implant fixture into the bone. Poor osseointegration of cementless implants is the leading clinical cause of implant loosening, subsidence, and arthroplasty failure, which

require costly and technically challenging revision surgery.[4] The mechanism of osseointegration requires further elucidation.

Vascular endothelial growth factor (VEGF) is one of the most important growth factors controlling vascular development and angiogenesis.[5] It also plays a crucial role in skeletal development and bone repair/regeneration and signals mainly via binding to VEGF receptor-1 (VEGFR-1) and VEGF receptor-2 (VEGFR-2).[6,7] Upon surgical placement, implants create a bone injury, and the mechanisms underlying their osseointegration appear similar to those occurring during bone repair and fracture healing. Following a fracture or placement of titanium implants in bone, a blood clot is formed and platelets release cytokines and growth factors including VEGF.[8–10] Thus, there is great interest in identifying cellular and molecular mechanisms of osseointegration by studying the role of VEGF in osseointegration. Recently, a specialized subset of vascular endothelium displaying high cell surface expression of CD31 and endomucin (EMCN; $CD31^{hi}EMCN^{hi}$ endothelium) has been reported to promote bone mass accrual and enhance fracture healing, raising the possibility that these cells are crucial targets of VEGF stimulation during osteogenesis or osseointegration.[11,12] However, the role of VEGF and $CD31^{hi}EMCN^{hi}$ endothelium during peri-implant bone healing is still largely unclear. We previously developed a novel mouse tibial implant that maintains *in vivo* knee joint function and provides an intra-articular and load-bearing environment for the study of osseointegration.[13] Here, we sought to understand the role of VEGF and $CD31^{hi}EMCN^{hi}$ endothelium in osseointegration using this model. Given the established angiogenic functions of VEGF, we hypothesized that blocking the VEGF pathway would also impair the skeletal specific elaboration of $CD31^{hi}EMCN^{hi}$ vascular endothelium in response to the implant.

Materials and Methods

Study design.

The experimental protocol was approved by our Institutional Animal Care and Use Committee. A total of 38, 16-week-old female C57BL/6 mice (Jackson Laboratory, Bar Harbor, Maine) underwent surgical implantation of a titanium implant in the right tibia. After the surgery, the animals were randomly divided into two groups: control group (n = 19) and anti-VEGFR group (n = 19). Intraperitoneal injections of 25 mg/kg of monoclonal antibodies MF1 (VEGFR-1 antibody, ImClone Systems, New York, New York) plus 25 mg/kg DC101 (VEGFR-2 antibody, ImClone Systems) in phosphate buffered saline (PBS) were administered for the anti-VEGFR group starting immediately after surgery and were given every third day until euthanasia. Isotype-matched control antibodies, which match the antibody characteristics but lack specificity of the target antigens, were administered to the control group. Flow cytometry and immunofluorescence were performed at two weeks post-surgery to quantitate and detect the spatial distribution of $CD31^{hi}EMCN^{hi}$ endothelium cells around the implant. Biomechanical testing was performed at four weeks post-implantation to determine the strength of the bone-implant interface.

Implant and surgical technique.

The mouse titanium implants were produced on a 3D direct metal laser sintering system (EOSINT M 270; EOS Electro Optical Systems, Munich, Germany). The implantation was performed as previously described.[13]

Fluorescence-activated cell sorting (FACS).

The right tibia (n = 4/group) was collected after the surrounding soft tissue was removed.[14,15] The proximal one-third tibia was crushed in Hanks Balanced Salt Solution (Life Technologies, Carlsbad, California) containing 10 mM HEPES (N-2-hydroxyethylpiperazine-N-2-ethane sulfonic acid, pH 7.2; Corning Life Sciences, Oneonta, New York) and enzymatically digested with 2.5 mg/ml Collagenase A (Roche, Basel, Switzerland) and 1 unit/ml Dispase II (Roche) for 15 minutes at 37°C under gentle agitation. The resulting cell suspensions were filtered (40 μm) and washed using PBS (pH 7.2) containing 0.5% bovine serum albumin (BSA; Fraction V, Sigma–Aldrich Corp, St Louis, Missouri) and 2 mM ethylenediaminetetraacetic acid (EDTA). After washing, equal numbers of cells per mouse were blocked with Purified Rat Anti-Mouse CD16/CD32 (BD Biosciences, San Jose, California) for 30 minutes on ice, then stained with allophycocyanin (APC)-conjugated EMCN antibody (eBioscience 50-5851-80), phycoerythrin (PE)-conjugated CD31 (eBioscience 12-0311-81), Alexa Fluor-conjugated CD45 (BioLegend 103128; Bio-Legend, San Diego, California), Brilliant Violet 711-conjugated CD146 (BD Biosciences 740827; BD Biosciences), and AP/Cy7-conjugated Ter119 (BioLegend 116223; BioLegend) for 45 minutes on ice. After washing, cells were resuspended in PBS (pH 7.2) with 2 mM EDTA and 1 μg/ml 4–6, diamidino-2-phenylindole (DAPI; live/dead exclusion) for analysis on an LSRII flow cytometer system (BD Biosciences) and analyzed using FlowJo software (TreeStar, Ashland, Oregon). Cell sorting was performed with an FACS Aria II SORP cell sorter (Becton Dickinson, Franklin Lakes, New Jersey) with exclusion of DAPI+ cells and doublets (Fig. 1).

Immunofluorescence.

For immunofluorescence, the right tibia (n = 3/group) was dissected immediately after euthanasia and fixed overnight in ice-cold 4% paraformaldehyde solution.[14,15] The bone samples were then kept in 5M EDTA at 4°C with constant shaking for 12 days for decalcification. All samples were embedded in OCT (optimal cutting temperature) compound, VWR Corporate, Radnor, Pennsylvania) and cut into 25 μm thick sagittal sections using a cryostat (Leica, Amsterdam, Netherlands). Immunofluorescence staining and analysis was performed as described previously.[16,17] Briefly, after treatment with 0.2% Triton X-100 (Sigma–Aldrich) for ten minutes, sections were blocked with 5% donkey serum at room temperature for 30 minutes and incubated overnight at 4°C with antibodies: CD31 (553370, BD Pharmingen, 1:100; BD Biosciences), CD31 conjugated to Alexa Fluor 488 (FAB3628G, R&D Systems, 1:50; R&D Systems, Minneapolis, Minnesota), EMCN (sc-65495, Santa Cruz, 1:100; Santa Cruz Biotechnology, Inc., Dallas, Texas), or beta-galactosidase antibody (GTX77365, GeneTex, 1:100; GeneTex, Inc., Irvine, California). Primary antibodies were visualized with species-appropriate Alexa Fluor-coupled secondary antibodies (1:400; Molecular Probes, Eugene, Oregon). Nuclei were counterstained with

DAPI. An Olympus IX81 confocal microscope (Olympus, Tokyo, Japan) or Zeiss LSM-880 confocal microscope (Carl Zeiss, Oberkochen, Germany) was used to image samples. Quantification of skeletal vasculature was performed as previously described.16 Briefly, the CD31-postive or EMCN-positive (red) area relative to the total basement membrane (BM) area (visualized in blue) was calculated using Image J software (open source; http://rsbweb.nih.gov/ij/).

To analyze the tissue on the implant surface, we scraped off tissue from the implant surface after pull-out testing at four weeks post-implantation. The tissue was pooled as the treated and control group, fixed in block, and cut into 25 μm-thick sagittal sections using a cryostat (Leica). After treatment with 0.2% Triton X-100 for ten minutes, sections were blocked with 5% donkey serum at room temperature for 30 minutes and incubated overnight at 4°C with antibodies: osteopontin (OPN; AF808, R&D Systems, 1:100; R&D Systems) and osterix (OSX; ab209484, Abcam Inc., 1:250; Abcam, Inc., Cambridge, Massachusetts). Primary antibodies were visualized with species appropriate Alexa Fluor-coupled secondary antibodies (1:400; Molecular Probes). Nuclei were counterstained with DAPI. An Olympus IX81 confocal microscope or Zeiss LSM-880 confocal microscope was used to image samples.

Biomechanical testing.

The strength of the bone-implant interface was measured with pull-out testing (n = 12/group). Specimens obtained at week four were wrapped in 0.9% saline solution-soaked gauze and were frozen at −20°C. Before testing, each tibia was thawed to room temperature. The distal end was potted in polymethylmethacrylate. Bone at the proximal end was dissected with a number-11 scalpel blade to allow the clamp of a custom fixture[18] to hold the implant beneath its plateau. Care was taken to minimize the amount of tissue removed and to not disturb the implant in the process. The long axis of the implant was aligned with the axis of pull-out loading. The implant was pulled out of the tibia at 0.03 mm/second under displacement to failure with an EnduraTEC ELF 3200 system (Bose, Eden Prairie, Minnesota). Maximum pull-out load (N) was calculated from the load-displacement curves.

RNA sequencing and analysis.

A total of 500 sorted $CD31^{hi}EMCN^{hi}$ endothelial cells were used for RNA sequencing (n = 3/group). One sample from each group was excluded due to the degradation of RNA. Total RNA (2.1 to 4.5 μg/mouse) was extracted using RNeasy Mini Kit (Qiagen, Hilden, Germany), and reverse transcription was performed with normalized amount of RNA using the High-Capacity cDNA Reverse Transcription Kit from Applied Biosystems (Foster City, California) according to the manufacturer's instructions.

The readings were aligned to the mm9 mouse genome (STAR version 2.3.0e)[19] using default parameters and resulting BAM files were sorted and indexed using the same tools. Gene counts were obtained by applying feature counts (version 1.4.3)[20] to sorted BAM files, and only unique-mapping readings were used. Genes without any expression counts in any sample were discarded. The DESeq2 (version 1.4.5) R package (Bioconductor)[21] was employed to normalize gene count data, and then detect differentially expressed genes

(DEGs) between anti-VEGFR treatment mice and control groups (false discovery rate < 0.1 and absolute log2 fold-change > 0.5). Mosaic version 1.1 was used to retrieve gene ontology (GO) information for all genes of the mouse genome.[22] Functional analysis was performed on DEGs using DAVID52 (version 6.7) and biological process GO terms with enrichment p < 0.05 were selected as overrepresented functions.

Statistical analysis.

Student's *t*-test was used to detect the difference between the anti-VEGFR and control group. A p-value < 0.05 was considered as significant.

Results

Both immunofluorescence and FACS revealed that anti-VEGFR treatment strongly decreased $CD31^{hi}EMCN^{hi}$ vascular endothelium in the peri-implant bone (Figs 2a to 2c). Furthermore, RNA sequencing transcriptional profiling demonstrated that the expression of a number of osteogenic factors such as bone morphogenetic protein 2 (BMP2) and fibroblast growth factor 2 (FGF2) in $CD31^{hi}EMCN^{hi}$ endothelial cells derived from implanted tibiae was reduced in anti-VEGFR treated mice relative to controls (Figs 2d and 2e). In summary, blocking VEGF signalling dramatically reduced the amount of $CD31^{hi}EMCN^{hi}$ vascular endothelium and its osteogenic ability during osseointegration.

At 28 days post-implantation, mechanical testing revealed that the maximum pull-out load of the implant in the anti-VEGFR group was 12.8 N (95% confidence interval (CI) 6.7 to 19.0), which was 35.7% lower than the value in the control group (19.9 N (95% CI 17.1 to 22.7); Fig. 3). Thus, post-implantation blockade of VEGF pathway significantly decreases mechanical strength of the bone-implant interface, indicating impaired osseointegration. No evidence of toxicity associated with anti-VEGFR treatment was observed, including no observable change in body weight (data not shown).

Consistent with decreased osteogenic factors derived from $CD31^{hi}EMCN^{hi}$ vascular endothelium after anti-VEGFR treatment, immunofluorescence showed that the treatment decreased both OPN- and OSX-positive cells in the peri-implant area at two weeks post-implantation (Fig. 4a). To further evaluate whether these decreases observed in the tissue were present on the implant surface, we isolated the peri-implant tissue that was attached to the implant surface after pull-out testing at four weeks (Fig. 4c). Immunofluorescence showed that anti-VEGFR treatment decreased OPN-positive cells while no OSX-positive cells were found in either group (Fig. 4b). Thus, the decrease of $CD31^{hi}EMCN^{hi}$ vascular endothelium caused by anti-VEGFR treatment is associated with a corresponding decrease in osteoblast-lineage cells.

Discussion

Bone repair following injury is usually a rapid and efficient process. Though osteoblasts are central to this process, other tissue types also present in bone, especially vascular endothelium, are also key participants. Thus, it is crucial to have temporal and spatial linkage of osteoblast activity with angiogenesis.[7,23,24] Most recently, osteoblast-derived slit

guidance ligand 3 (SLIT3) has been identified as a key factor linking osteoblast activity to the formation of $CD31^{hi}EMCN^{hi}$ endothelium at sites of osteoanabolic activity.[15] The manner in which angiogenesis and osteoanabolic responses are linked in the context of osseointegration of orthopaedic implants is still unclear. Similar to trauma or fractures, surgical insertion of implants creates a bone injury. However, it is not known how similar the mechanisms of implant osseointegration are to those of bone repair and fracture healing. In the present study, we used a murine model of osseointegration of an intra-articular titanium implant that was loaded through the knee joint and supported by the cancellous bone bed of the proximal tibia[13] to test the hypothesis that blocking of VEGF signalling impairs osseointegration and leads to a decrease in the peri-implant elaboration of $CD31^{hi}EMCN^{hi}$ endothelium.

Indeed, blockade of VEGF signalling decreased osseointegration and $CD31^{hi}EMCN^{hi}$ endothelium in the peri-implant bone. These findings are broadly consistent with other studies suggesting the linkage between osteogenesis and angiogenesis,[6] especially with respect to $CD31^{hi}EMCN^{hi}$ vessels.[12]

Bimodality was present in the maximum pull-out load but did not correlate with radiological placement of the implant or other parameters. Therefore, we cannot exclude that this simply represents a response pattern produced by experimental variation.

Furthermore, blockade of VEGF signalling decreased the expression of osteogenic factors such as BMP2 and FGF2 in isolated $CD31^{hi}EMCN^{hi}$ cells and correspondingly decreased the density of the OPN- or OSX-positive osteoblast lineage cells in the peri-implant bone. This suggests a model whereby osteoprogenitor cells differentiating into bone-forming osteoblasts preferentially associate with $CD31^{hi}EMCN^{hi}$ endothelial cells as a source of several growth factors relevant for the survival and proliferation of osteoprogenitors.[11] Although $CD31^{hi}EMCN^{hi}$ cells are relatively rare in number, $CD31^{hi}EMCN^{hi}$ endothelium and the osteoblast lineage cells' physical proximity may act to amplify each other's physiological effects.[15] Importantly, VEGF has pleiotropic effects on several cell types in the skeleton,[7] raising the possibility that, in addition to its angiogenic roles, VEGF may have direct effects on mesenchymal cells in addition to effects on $CD31^{hi}EMCN^{hi}$ vessels.

To confirm that VEGF pathway controls the coupling of angiogenesis and osteogenesis during implant osseointegration, it is important to measure the bone-implant contact area and the abundance of blood vessels in the peri-implant region directly; however, the current technologies available pose limitations in trying to examine this bone-implant region. Some limitations are the beam hardening effects around metal surfaces in micro CT, difficulty of precise cutting and grinding of samples with metal for histomorphometric analysis, and the challenge of visualizing vessels of small calibre with an angiograph.

Cementless total joint arthroplasties provide superior long-term fixation compared with conventional cemented implants.[25] However, such implants can fail due to implant movement, inflammation and bone resorption, and osteolysis caused by poor osseointegration, leading to costly and technically challenging revision surgery.[26] From this perspective, developing a means for medical therapy to promote early osseointegration

would be valuable. These data suggest that supplementation of exogenous VEGF or modulation of VEGF signalling should be further explored as a means to enhance osseointegration. In addition, we have here developed a system to run flow cytometric analysis and perform immunofluorescent staining on the limited tissue around the implant in this mouse model. This will be a powerful platform for future mechanistic studies on osseointegration.

Acknowledgements:

This study was supported by the Complex Joint Reconstruction Center at Hospital for Special Surgery and Feldstein Medical Foundation.

Funding statement:

M. B. Greenblatt is supported by DP5OD021351 from the Office of the Director of the National Institutes of Health (NIH) and holds a Career Award for Medical Scientists from the Burroughs Welcome Foundation.

No benefits in any form have been received or will be received from a commercial party related directly or indirectly to the subject of this article.

References

1. Perren SM. Evolution of the internal fixation of long bone fractures. The scientific basis of biological internal fixation: choosing a new balance between stability and biology. J Bone Joint Surg [Br] 2002;84-B:1093–1110.
2. Chong DY, Hansen UN, Amis AA. Analysis of bone-prosthesis interface micromotion for cementless tibial prosthesis fixation and the influence of loading conditions. J Biomech 2010;43:1074–1080. [PubMed: 20189576]
3. Brånemark PI, Hansson BO, Adell R, et al. Osseointegrated implants in the treatment of the edentulous jaw. Experience from a 10-year period. Scand J Plast Reconstr Surg Suppl 1977;16:1–132. [PubMed: 356184]
4. Lee K, Goodman SB. Current state and future of joint replacements in the hip and knee. Expert Rev Med Devices 2008;5:383–393. [PubMed: 18452388]
5. Coultas L, Chawengsaksophak K, Rossant J. Endothelial cells and VEGF in vascular development. Nature 2005;438:937–945. [PubMed: 16355211]
6. Zelzer E, McLean W, Ng YS, et al. Skeletal defects in VEGF(120/120) mice reveal multiple roles for VEGF in skeletogenesis. Development 2002;129:1893–1904. [PubMed: 11934855]
7. Hu K, Olsen BR. Osteoblast-derived VEGF regulates osteoblast differentiation and bone formation during bone repair. J Clin Invest 2016;126:509–526. [PubMed: 26731472]
8. Al Subaie AE, Eimar H, Abdallah MN, et al. Anti-VEGFs hinder bone healing and implant osseointegration in rat tibiae. J Clin Periodontol 2015;42:688–696. [PubMed: 26073407]
9. Davies JE. Understanding peri-implant endosseous healing. J Dent Educ 2003;67:932–949. [PubMed: 12959168]
10. Eriksson C, Nygren H, Ohlson K. Implantation of hydrophilic and hydrophobic titanium discs in rat tibia: cellular reactions on the surfaces during the first 3 weeks in bone. Biomaterials 2004;25:4759–4766. [PubMed: 15120522]
11. Kusumbe AP, Ramasamy SK, Adams RH. Coupling of angiogenesis and osteogenesis by a specific vessel subtype in bone. Nature 2014;507:323–328. [PubMed: 24646994]
12. Ramasamy SK, Kusumbe AP, Wang L, Adams RH. Endothelial Notch activity promotes angiogenesis and osteogenesis in bone. Nature 2014;507:376–380. [PubMed: 24647000]
13. Yang X, Ricciardi BF, Dvorzhinskiy A, et al. Intermittent parathyroid hormone enhances cancellous osseointegration of a novel murine tibial implant. J Bone Joint Surg [Am] 2015;97-A:1074–1083.

14. Xu R, Yallowitz A, Qin A, et al. Targeting skeletal endothelium to ameliorate bone loss. Nat Med 2018;24:823–833. [PubMed: 29785024]
15. Yin H, Huang J, Cao X, et al. Inhibition of Src homology 2 domain-containing protein tyrosine phosphatase-2 facilitates CD31hiEndomucinhi blood vessel and bone formation in ovariectomized mice. Cell Physiol Biochem 2018;50:1068–1083. [PubMed: 30355920]
16. Fukuda T, Takeda S, Xu R, et al. Sema3A regulates bone-mass accrual through sensory innervations. Nature 2013;497:490–493. [PubMed: 23644455]
17. Xu R, Zhang C, Shin DY, et al. c-Jun N-terminal kinases (JNKs) are critical mediators of osteoblast activity in vivo. J Bone Miner Res 2017;32:1811–1815. [PubMed: 28561373]
18. Zhang L, Jia TH, Chong AC, et al. Cell-based osteoprotegerin therapy for debris-induced aseptic prosthetic loosening on a murine model. Gene Ther 2010;17:1262–1269. [PubMed: 20428210]
19. Dobin A, Davis CA, Schlesinger F, et al. STAR: ultrafast universal RNA-seq aligner. Bioinformatics 2013;29:15–21. [PubMed: 23104886]
20. Liao Y, Smyth GK, Shi W. featureCounts: an efficient general purpose program for assigning sequence reads to genomic features. Bioinformatics 2014;30:923–930. [PubMed: 24227677]
21. Love MI, Huber W, Anders S. Moderated estimation of fold change and dispersion for RNA-seq data with DESeq2. Genome Biol 2014;15:550. [PubMed: 25516281]
22. Zhang C, Hanspers K, Kuchinsky A, et al. Mosaic: making biological sense of complex networks. Bioinformatics 2012;28:1943–1944. [PubMed: 22576176]
23. Maes C, Goossens S, Bartunkova S, et al. Increased skeletal VEGF enhances beta-catenin activity and results in excessively ossified bones. EMBO J 2010;29:424–441. [PubMed: 20010698]
24. Park D, Spencer JA, Koh BI, et al. Endogenous bone marrow MSCs are dynamic, fate-restricted participants in bone maintenance and regeneration. Cell Stem Cell 2012;10:259–272. [PubMed: 22385654]
25. Newman JM, Sodhi N, Dekis JC, et al. Survivorship and functional outcomes of cementless versus cemented total knee arthroplasty: a meta-analysis. J Knee Surg 2019 (Epub ahead of print)
26. Berry DJ, Wold LE, Rand JA. Extensive osteolysis around an aseptic, stable, uncemented total knee replacement. Clin Orthop Relat Res 1993;293:204–207.

Take home message

- Vascular endothelial growth factor (VEGF) is critical to achieving early osseointegration.
- The positive result will warrant more studies on pro-VEGF agents as target agents to enhance osseointegration in patients receiving a cementless implant.

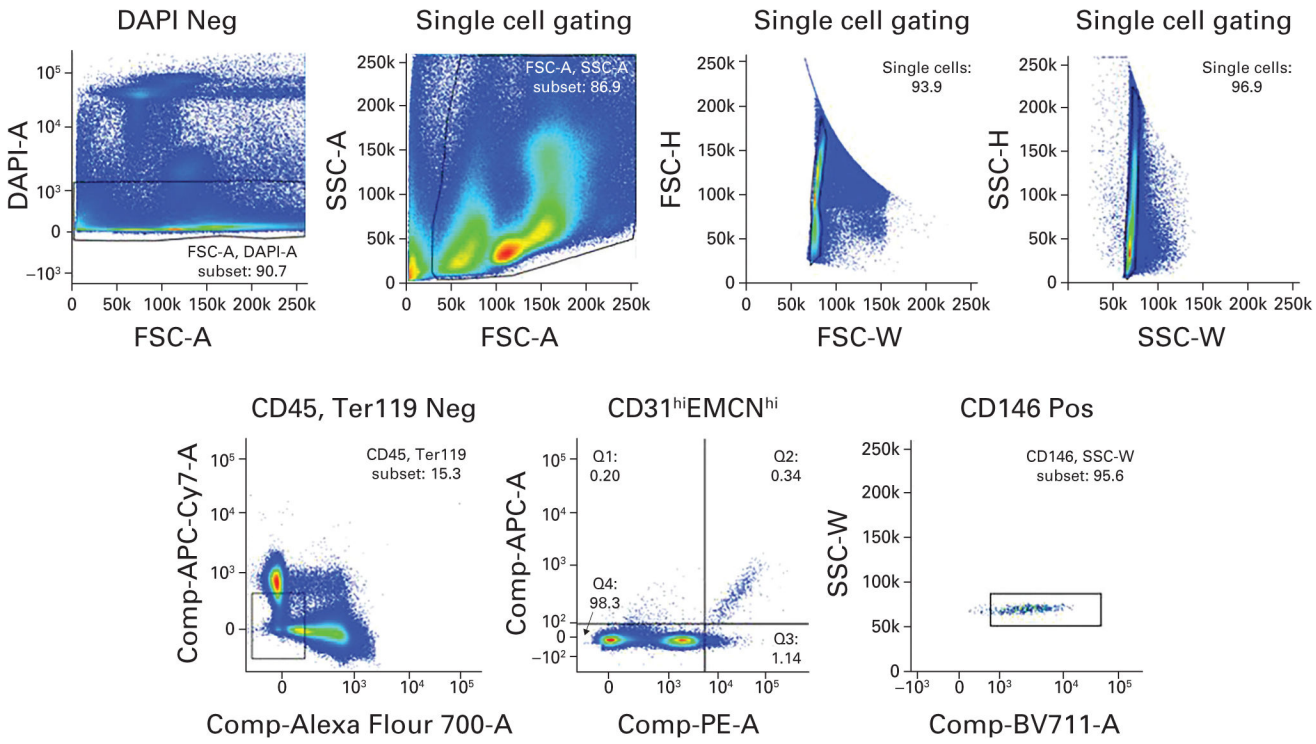

Fig. 1.

The strategy used for flow cytometry for analysis of CD31^{hi}EMCN^{hi} endothelial cells. DAPI, diamidino-2-phenylindole; FSC, forward scatter; SSC, side scatter; APC, allophycocyanin.

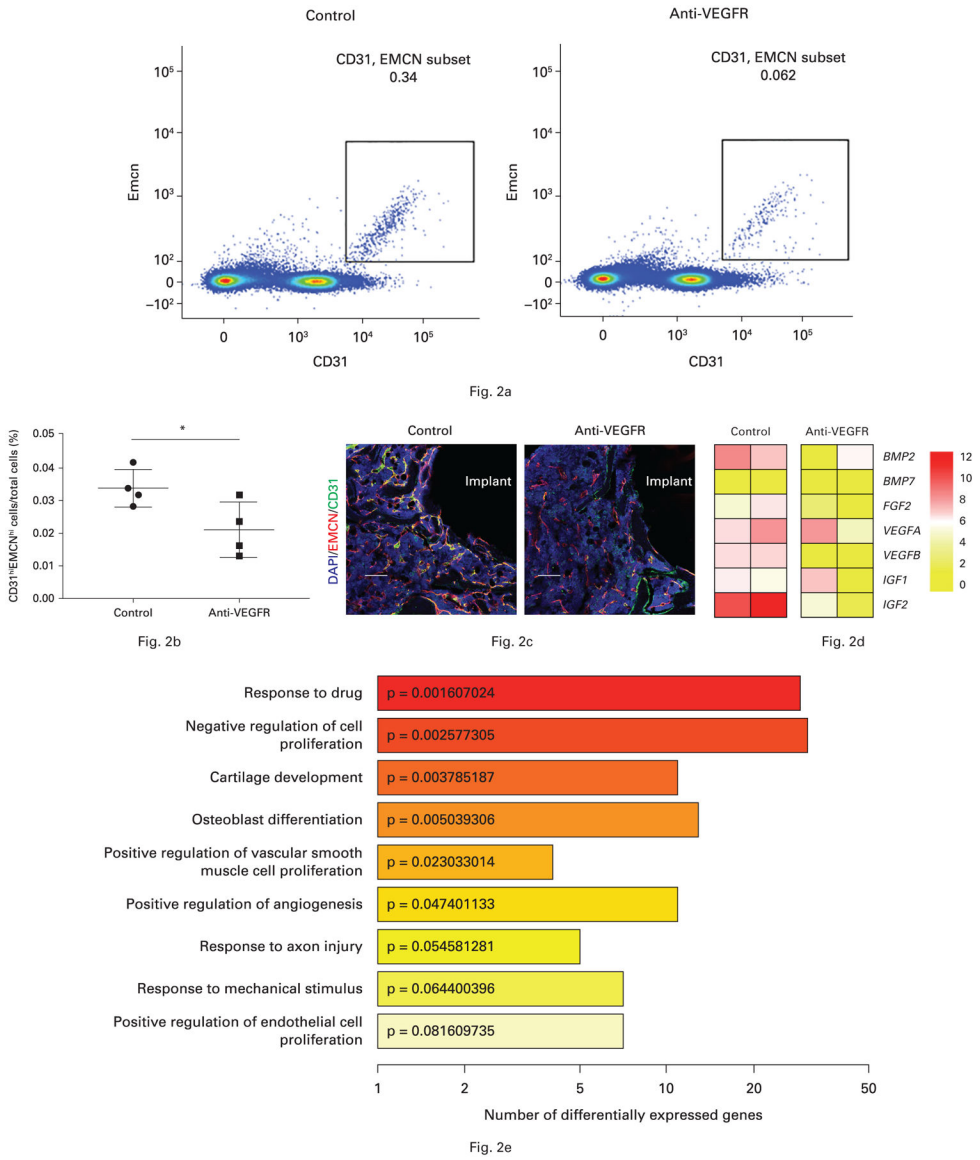

Fig. 2.

a) and b) Anti-vascular endothelial growth factor receptor (VEGFR) treatment decreased the number of $CD31^{hi}EMCN^{hi}$ cells in peri-implant bone detected by flow cytometry (the middle line indicates the mean, and the other two lines represent the standard deviation). c) Anti-VEGFR treatment decreased the CD31 and endomucin (EMCN) double-positive cells (yellow) detected by immunofluorescence. d) Anti-VEGFR inhibited bone morphogenetic protein 2 (BMP2) and insulin-like growth factor 2 (IGF2) expressions in these sorted $CD31^{hi}EMCN^{hi}$ cells. e) Gene ontology (GO) enrichment analysis of differentially expressed genes between control mice and anti-VEGFR treated mice. Each bar is coloured and labelled according to p-value of enrichment analysis. *$p < 0.05$. Scale bar: 250 μm. DAPI, diamidino-2-phenylindole; FGF2, fibroblast growth factor 2.

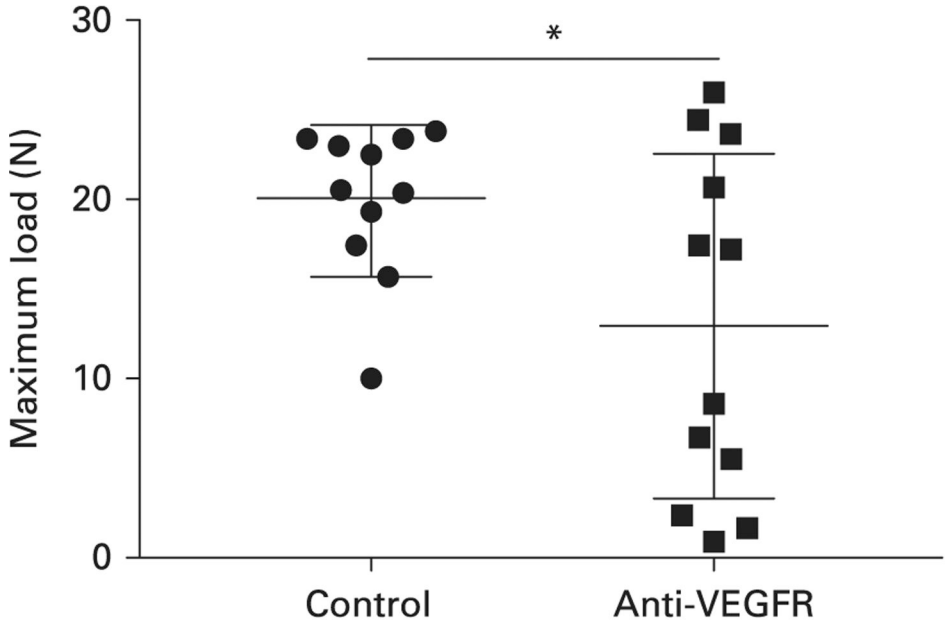

Fig. 3.

Anti-vascular endothelial growth factor receptor (VEGFR) treatment decreased the maximum load of pull-out testing (the middle line indicates the mean, and the other two lines represent the standard deviation). *p = 0.036.

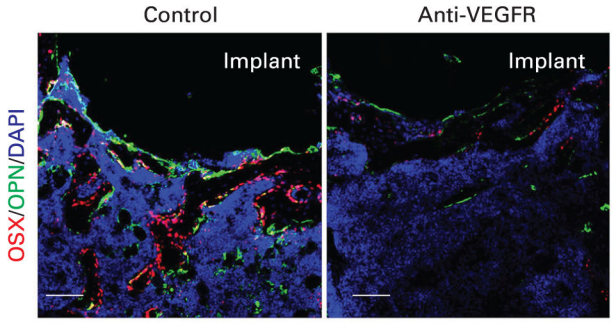

Fig. 4a

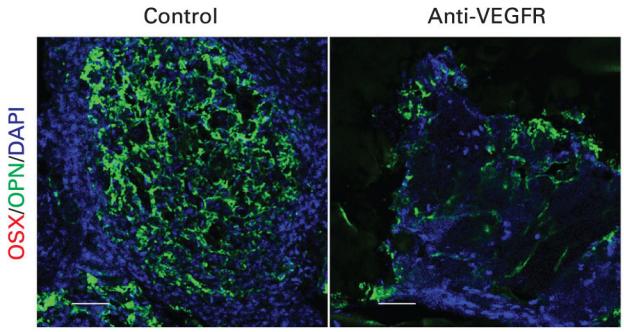

Fig. 4b

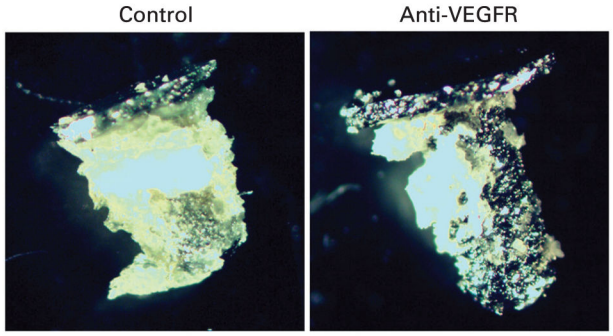

Fig. 4c

Fig. 4.

a) Anti-vascular endothelial growth factor receptor (VEGFR) treatment decreased osteopontin (OPN) and osterix (OSX) in peri-implant tissue at two weeks post-implantation. b) The treatment also decreased OPN in tissue on implant surface at four weeks. c) Representative image of tissue on implant surface. Scale bar: 250 μm. DAPI, diamidino-2-phenylindole.